Supporting information

Orange–Red Si Quantum Dot LEDs from Recycled Rice Husks

Shiho Terada[a], Honoka Ueda[b], Taisei Ono[a], Ken-ichi Saitow[a,b,c]*

[a] Department of Chemistry, Graduate School of Science, Hiroshima University, 1-3-1 Kagamiyama, Higashi-Hiroshima, Hiroshima 739-8526, Japan

[b] Graduate School of Advanced Science and Engineering, Hiroshima University, 1-3-1 Kagamiyama, Higashi-Hiroshima, Hiroshima 739-8526, Japan

[c] Department of Materials Science, Natural Science Center for Basic Research and Development (N-BARD), Hiroshima University, 1-3-1 Kagamiyama, Higashi-hiroshima, Hiroshima 739-8526, Japan

Contents:

SI 1. SEM images and size analyses of Si particles before and after grinding

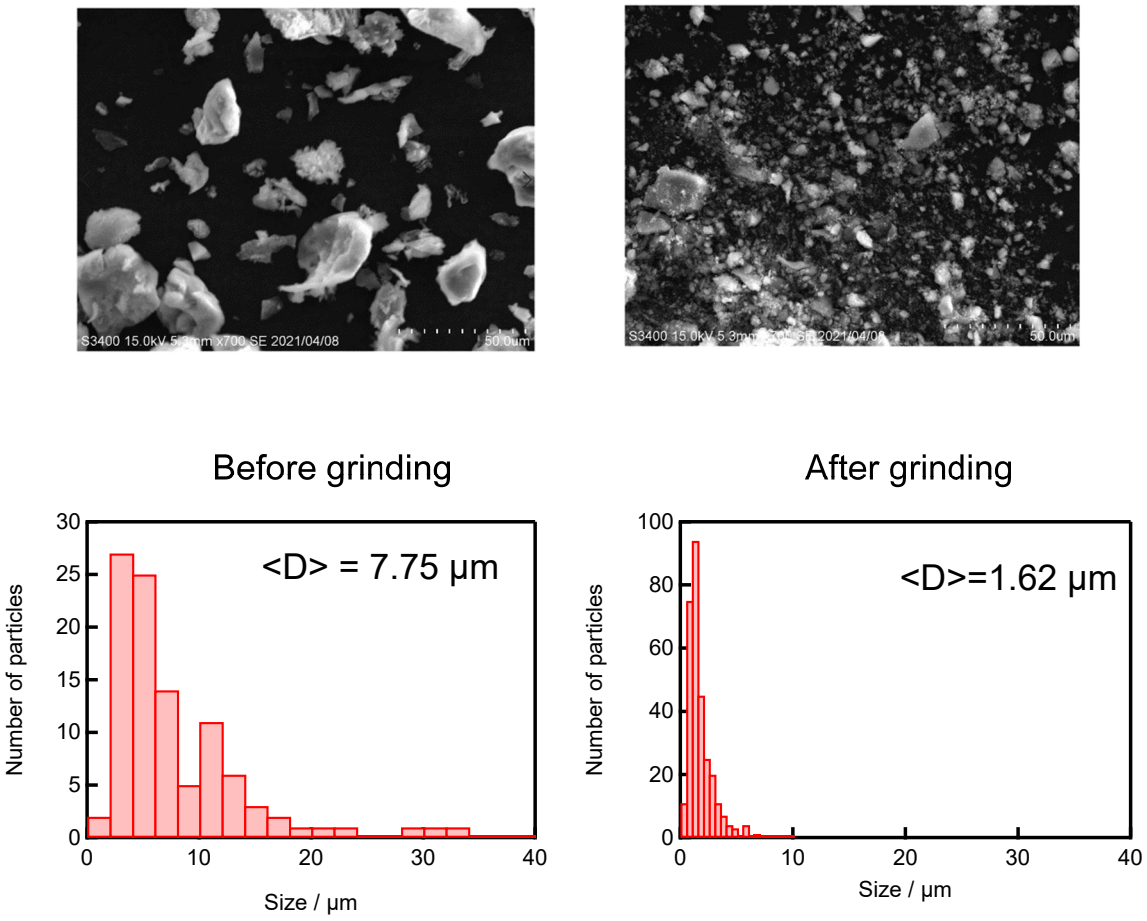

Figure S1. Typical SEM images of Si particles obtained from RHs and their size analyses. Left and right sides represent the data of Si particles before and after grinding with a motor and pastel, respectively.

SI 2. Chemical and physical structures of Si obtained from rice husk

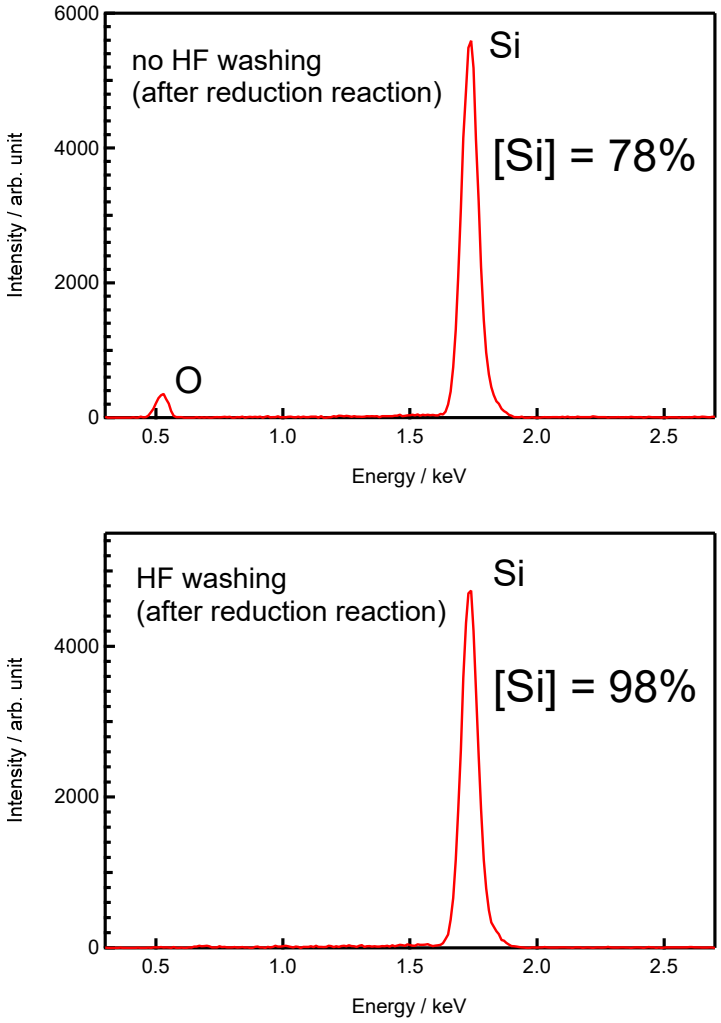

Figure S2. EDX spectra to evaluate the purity of Si particles obtained from RHs. Residual silica components were involved in Si particles after the reduction reaction, and they were removed by HF washing. The purity of Si increased to 98%.

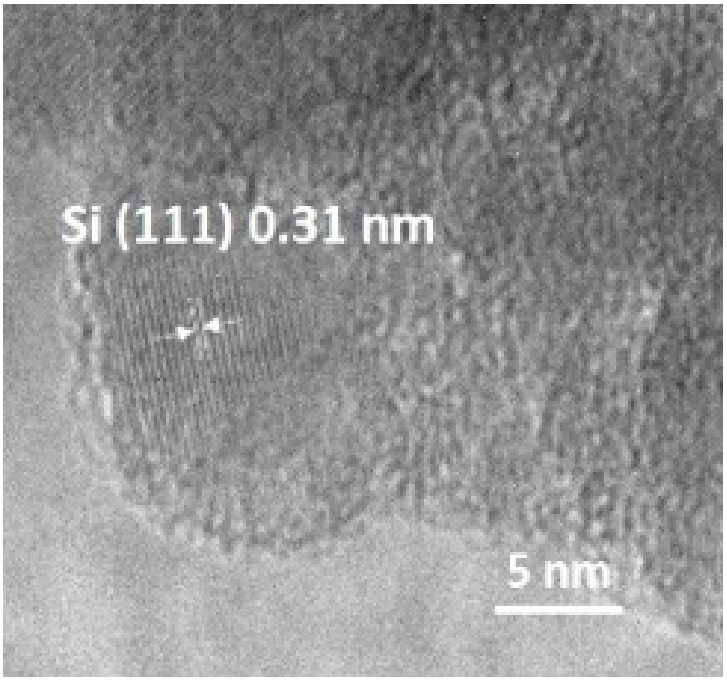

Figure S3. HRTEM image of Si nanoparticles synthesized from RHs after chemical etching. The data denotes the expanded image of Figure 1k for the clarity.

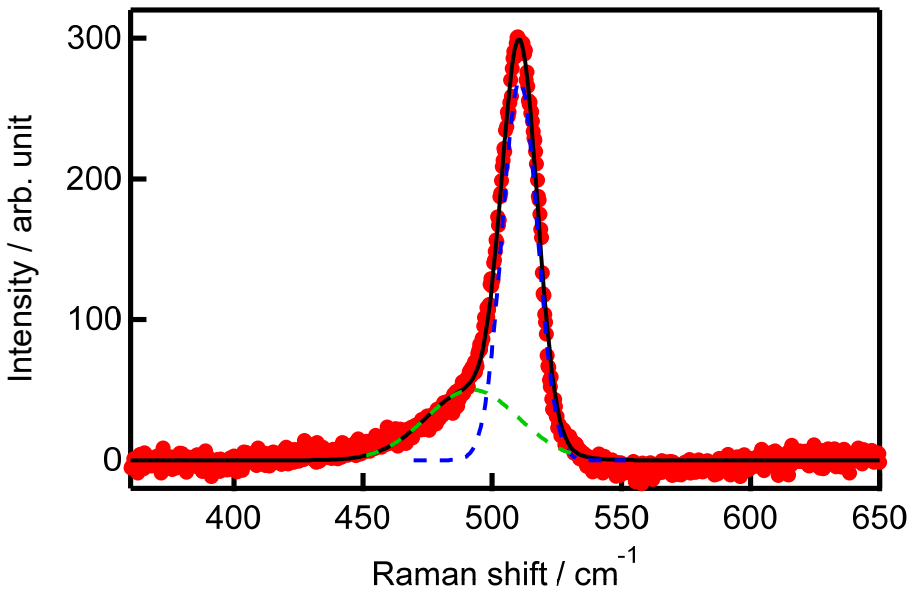

Figure S4. Raman spectrum of H-SiQD measured upon an excitation wavelength of 632.8 nm. Red solid circles and a black solid curve denote raw data and fitting curve of two Gaussian functions, respectively. Blue and green dashed curve denote crystalline and amorphous components, respectively. According to the relative area, crystalline and amorphous components of H-SiQDs were estimated as 63±3 % and 37±3%, respectively, both of which average and standard deviations were obtained from six Raman spectra.

SI 3. PL of SiQD changed by etching time

The Si particle solution was chemically etched with HF and HNO_3 solutions to remove the oxidized surface layer of SiO_2 and to reduce the particle size.[1] The PL color of obtained H-SiQDs was changed by etching conditions. Successively, H-SiQDs were used to synthesize de-SiQDs as a final product. Herein, we show the different PL spectra by changing etching time to synthesize H-SiQDs. This is because PL wavelength is modified by quantum confinement effect (Figure S6). Figure S5 shows the PL spectra of de-SiQDs, and their peak wavelengths were changed by etching time for synthesizing H-SiQDs.

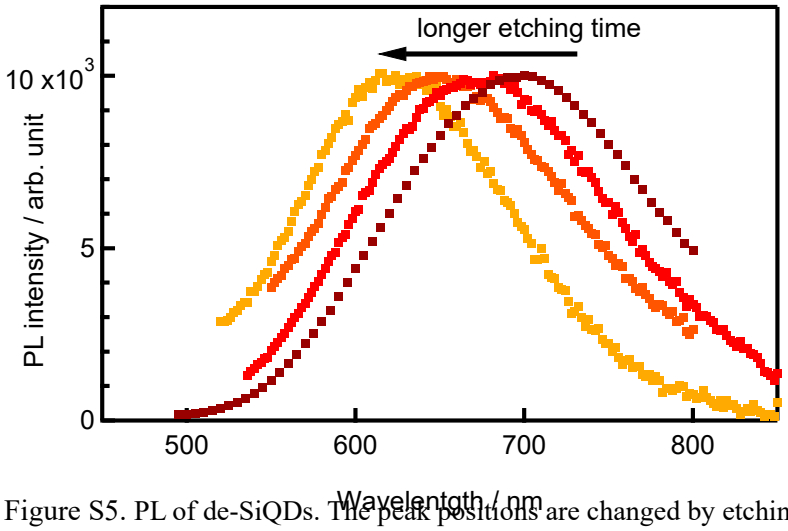

Figure S5. PL of de-SiQDs. The peak positions are changed by etching time.

SI 4. Band gap energy and EMA of SiQDs

The bandgap energy (E_g) of SiQD depends on the size, and their values can be analyzed by quantum confinement effect.[2-4] That is, the energy of the PL peak has been used as an indication of E_g for Si nanomaterials. The quantum-confinement effect of Si nanomaterials shows the relationship between E_g and d (diameter of SiQD) with the effective mass approximation (EMA) as follows,[2-4]

$$E_{QD} = E_0 + \frac{h^2\pi^2}{2d^2}\left(\frac{1}{m_e^*} + \frac{2}{m_h^*}\right) - \frac{1.786e^2}{\varepsilon d} \quad (1)$$

where E_{QD} is the bandgap of SiQD, E_0 bulk Si (1.12 eV), d diameter of SiQD, m_e^* effective mass of electron, m_h^* effective mass of hole, ε dielectric constant of Si.

The equation of (1) is characterized for SiQDs using eq. (2).

$$E_{QD} = E_0 + Ad^{-2} - Bd^{-1} \quad (2)$$

where A and B are constants and lead to A = 2.56 eV nm $^{-2}$ and B = 0.83 eV nm $^{-1}$.[3] The units of E and d are eV and nm, respectively. Based on eq. (2), we obtained a solid curve in Figure S6. Symbols are collected from recent papers for peak wavelengths of PL spectra of colloidal SiQDs.[2-11] The orange square represents the de-SiQD synthesized in the present study (E_g=1.8 eV, diameter = 3.5 nm). Thus, the position of PL wavelength and E_g for the present de-SiQDs were specified by the quantum-confinement effect and EMA.

Herein, let us describe other two information. First, it is the deviation between experimental data and EMA curve in the size < 2 nm, which is well described by recent study.[2] That is, the dispersion of particle size distribution is responsible for the deviation between experimental data and EMA. In other words, if one can synthesize the SiQD with small standard deviation for size distribution, the experimental data will be good agreement

with EMA in the size < 2 nm.[3] Second, almost green-blue PL reported in studies on Si nanomaterials are commonly linked to radiative defects. The interband transition and radiative defects have been attributed S-band and F-band, respectively, and summarized in recent review articles.[3,4]

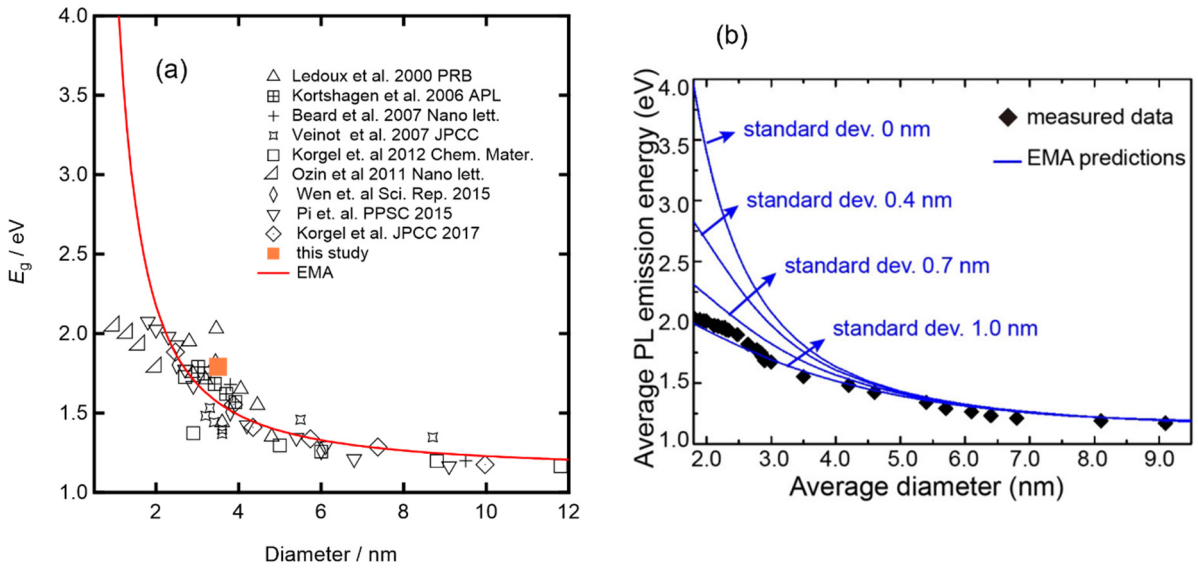

Figure S6. E_g obtained from PL peak wavelengths of colloidal SiQDs. (a) Symbols and sold curve are obtained from papers (refs. 2-11) and calculations of EMA, respectively. Orange square is the data in the present study in the present study (E_g=1.8 eV, diameter = 3.5 nm). (b) Figure is reused from ref. 2 (Copyright in American chemical society). The deviation from EMA is characterized by the standard deviation of SiQD size.

SI 5. Performance of SiQD LEDs

We evaluated the performance of SiQD LED. Figure S7 shows an *I-V* curve of SiQD LED, which was prepared using another device with the same structure to SiQD LED in Figure 3. The external quantum efficiency (EQE) of SiQD LED was estimated using equation (3).

$$\mathrm{EQE}\ [\%] = \frac{\frac{\text{Optical power density}\ [\mathrm{W/cm^2}]}{\text{Single photon energy}\ [\mathrm{J}]}}{\frac{\text{Current density}\ [\mathrm{A/cm^2}]}{\text{Elementary charge}\ [\mathrm{C}]}} \times 100 \qquad (3).$$

The obtained EQE was calibrated by considering light correction efficiency, based on a reported manner.[12] The resultant maximum EQE was obtained as 0.003%. This value was lower than the typical EQE for SiQD LEDs (Table S1). Namely, the maximum EQE reported for SiQD LEDs is 8.6%, with ranges from 1 to 4% at their optimized voltages, although lower EQEs of 0.02-0.6 % are prevalent, depending on the applied voltage and the device structure (Table S1).[14-26] A future requirement is to enhance EQE of SiQD LED derived from rice husks.

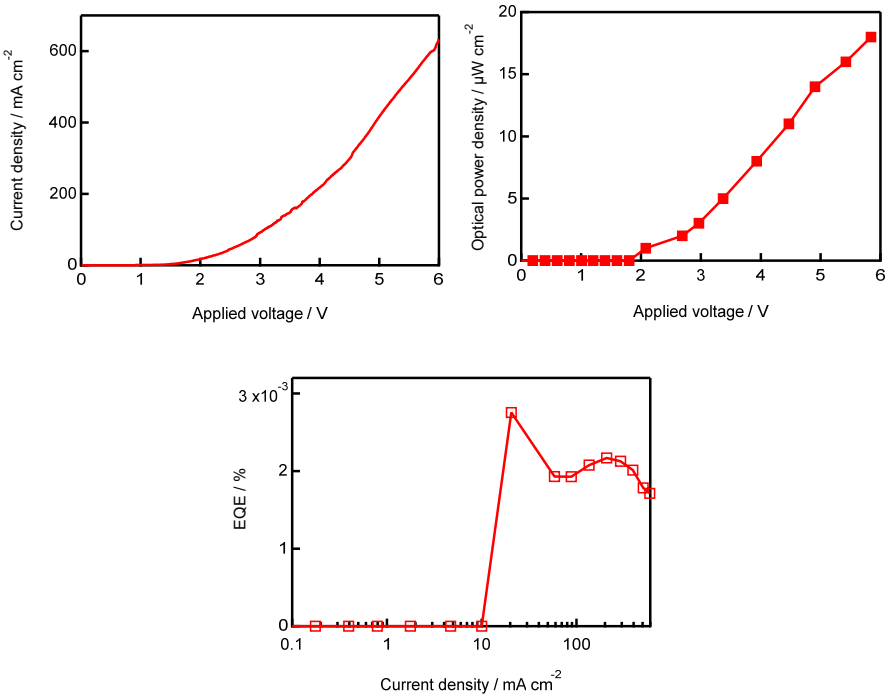

Figure S7. Performance of SiQD LED.

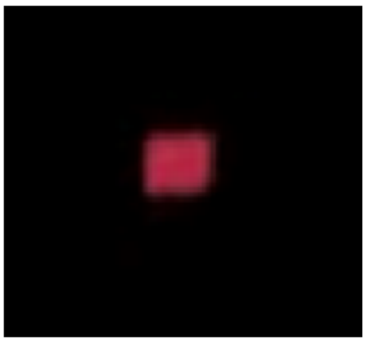

Figure S8. Photograph of SiQD LED working, of which performance is shown in Figure S7. EL peak wavelength was located at 700 nm. The size of active area was 2 mm × 2 mm.

Table S1. Device structures and external quantum efficiencies of SiQD LEDs

Year	Device structure[a]	EL peak wavelength (nm)	maximum EQE (%)	EQE[b] (%)	ref.
2010	ITO/PEDOT:PSS/MEH-PPV/SiQD/BCP/LiF/Al	868	0.6	0.01 – 0.4	14
2011	ITO/PEDOT:PSS/Poly-TPD/SiQDs/TiO_2/Al	618	---	0.00001	15
2011	ITO/PEDOT:PSS/Poly-TPD/SiQDs/Alq_3/LiF/Al	853	8.6	0.01 – 6.5	16
2011	ITO/PVK/SiQD/TPBi/Al	685	0.7	0.01 – 0.4	17
2013	ITO/PEDOT:PSS/Poly-TPD/SiQD/TPBi/LiF/Al	680	1.1	0.0001 – 0.02	18
2015	ITO/PEDOT:PSS/Poly-TPD/SiQDs/Alq_3/Al	410	---	0.00042	12
2016	Al/MoO_3//TAPC/SiQD/ZnO/PEI/ITO (inverted structure)	690	2.7	0.03 – 1	19
2018	Al/MoO_3/CBP/SiQD/ZnO/ITO (inverted structure)	660	3.1	0.2 – 2	20
2018	ITO/PEDOT:PSS/Poly-TPD/SiQD/ZnO/Ca/Al	694	0.018	0.001 - 0.007	21
2018	ITO/PEDOT:PSS/Poly-TPD/PVK/SiQD/ZnO/Ag	735	6.2	0.1 – 3.5	22
2018	ITO/PEDOT:PSS/SiQD/TPBi/Al	700	0.3	0.02 – 0.2	23
2018	Au/MoO_3/CBP/SiNC/ZnO/ITO (inverted structure)	740	3	0.5 – 1.5	24
2019	Al/MoO_3/CBP/SiQD/ZnO/ITO (inverted structure)	620	0.03	0.01 – 0.025	25
2019	Al/WO_3/SiQD/ZnO/ITO (inverted structure)	680	0.25	0.001 – 0.2	26
2020	Al/MoO_3/CBP/SiQD/ZnO/ITO (inverted structure)	755	3.36	0.01 – 1	13

a: The device structures are listed from anode at the left side to cathode at the right side.
b: The EQEs are listed as the values at non-optimized voltages, indicating 70% data except for the top 30% EQE at optimized voltages. Their average was obtained as 0.02-0.6% by excluding the highest three EQEs and the lowest three EQE in the right column.

SI 6. Improvements of de-SiQD synthesis

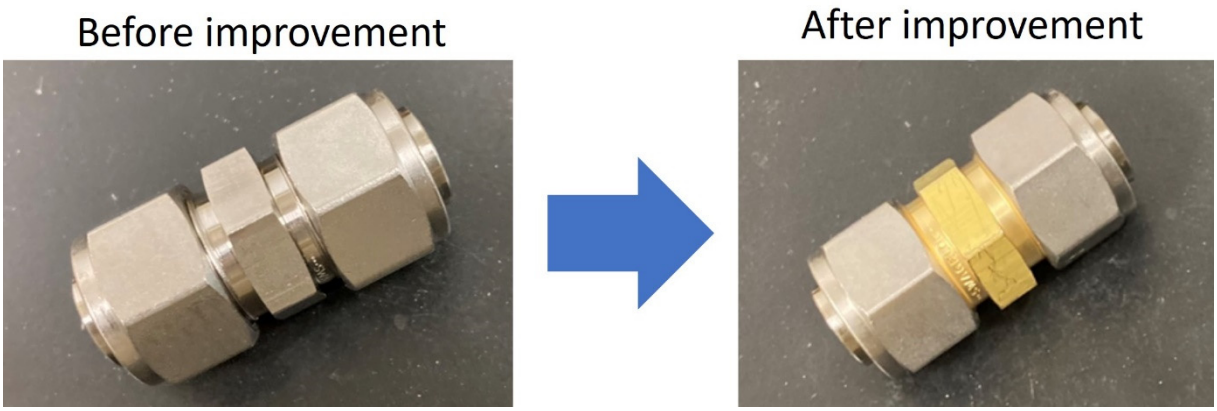

Figure S9. Photographs of reaction vessels using commercial Swagelok parts (5/8 inch). The left and right photographs are reaction vessels before and after improvement, respectively. The body and screw caps of former were made of stainless steel, whereas those of latter were made of brass and stainless steel, respectively. Using materials with different coefficient of thermal expansion, we reduced a burn-in between the screw cap of the reaction vessel without the lubricant, and the lubricant involving Ag was not necessary. This latter type of the vessel was also used in ref. 27.

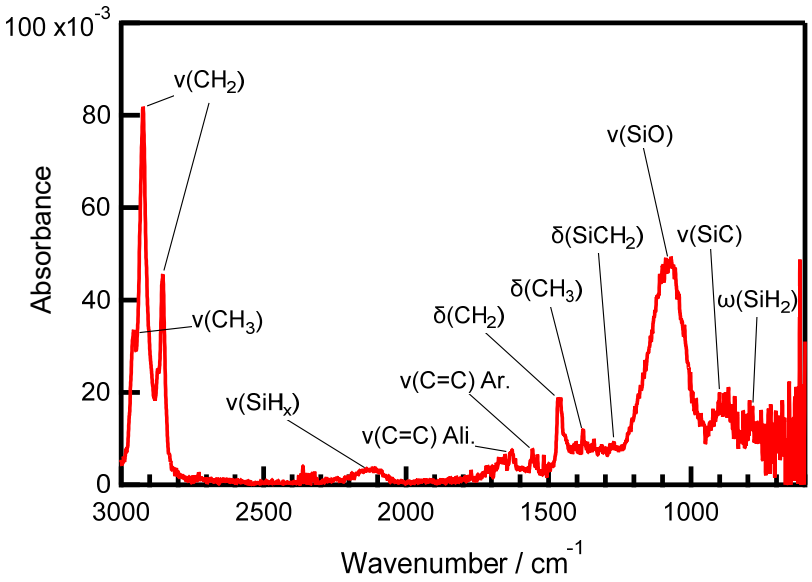

Figure S10. FTIR spectrum of improved de-SiQDs, corresponding to Ag free and negligible surface contaminants. Notations of ν, δ, and ω denote stretching, scissoring, and wagging modes, respectively.

SI. 7 References

1. Sato, K.; Tsuji, H.; Hirakuri, K.; Fukata, N.; Yamauchi, Y. Controlled Chemical Etching for Silicon Nanocrystals with Wavelength-Tunable Photoluminescence, Chem. Commun., 2009, 3759–3761.
2. Yu, Y.; Fan, G.; Fermi, A.; Mazzaro, R.; Morandi, V.; Ceroni, P.; Smilgies, D.; Korgel, B. Size-Dependent Photoluminescence Efficiency of Silicon Nanocrystal Quantum Dots. J. Phys. Chem. C 2017, 121, 23240–23248.
3. Liu, X.; Zhang, Y.; Yu, T.; Qiao, X.; Gresback, R.; Pi, X.; Yang, D. Optimum Quantum Yield of the Light Emission from 2 to 10 nm Hydrosilylated Silicon Quantum Dots, Part. Part. Syst. Charact. 2016, 33, 44–52.
4. Canham, L., Introductory Lecture: Origins and Applications of Efficient Visible Photoluminescence from Silicon-Based Nanostructures, Faraday Discuss., 2020, 222, 10-81.
5. Beard, M. C.; Knutsen, K. P.; Yu, P.; Luther, J. M.; Song, Q.; Metzger, W. K.; Ellingson, R. J.; Nozik, A. J. Multiple Exciton Generation in Colloidal Silicon Nanocrystals. Nano Lett. 2007, 7, 2506– 2512.
6. Hessel, C. M. ; Reid, D. ; Panthani, M. G.; Rasch, M.R.; Goodfellow, B. W.; Wei, J. W.; Fujii, H.; Akhavan, V.; Korgel, B. A. Synthesis of Ligand-Stabilized Silicon Nanocrystals with Size-Dependent Photoluminescence Spanning Visible to Near-Infrared Wavelengths, Chem. Mater. 2012, 24, 393-401.
7. Jurbergs, D.; Rogojina, E.; Mangolini, L.; Kortshagen, U. Silicon Nanocrystals with Ensemble Quantum Yields Exceeding 60%, Appl. Phys. Lett. 2006, 88, 233116/1-233116/3.
8. Ledoux, G.; Guillois, O.; Porterat, D.; Reynaud, C.; Huisken, F.; Kohn, B.; Paillard, V. Photoluminescence Properties of Silicon Nanocrystals as a Function of their Size, Phys. Rev. B. 2000, 62, 15942–15951.
9. Mastronardi, M. L.; Maier-Flaig, F.; Faulkner, D.; Henderson, E. J.; Kubel, C.; Lemmer, U.; Ozin, G. A. Size-Dependent Absolute Quantum Yields for Size-Separated Colloidally-Stable Silicon Nanocrystals. Nano Lett. 2012, 12, 337–342.
10. Hessel, C. M.; Henderson, E. J.; Veinot, J. G. C. An Investigation of the Formation and Growth of Oxide-Embedded Silicon Nanocrystals in Hydrogen Silsesquioxane-Derived

Nanocomposites. J. Phys. Chem. C 2007, 111, 6956– 6961.

11. Wen, X.; Zhang, P.; Smith, T. A.; Anthony, R. J.; Kortshagen, U. R.; Yu, P.; Feng, Y.; Shrestha, S.; Coniber, G.; Huang, S. Tunability Limit of Photoluminescence in Colloidal Silicon Nanocrystals, Sci. Rep. 2015, 5, 12469.
12. Xin, Y.; Nishio, K.; Saitow, K. White-Blue Electroluminescence from a Si Quantum Dot Hybrid Light-Emitting Diode. *Appl. Phys. Lett.* **2015**, *106*, 201102.
13. Yamada, H.; Saitoh, N.; Ghosh, B.; Masuda, Y.; Yoshizawa, N.; Shirahata, N. Improved Brightness and Color Tunability of Solution-Processed Silicon Quantum Dot Light-Emitting Diodes. J. Phys. Chem. C 2020, 124, 23333–23342.
14. Cheng, K.-Y.; Anthony, R.; Kortshagen, U. R.; Holmes, R. J. Hybrid Silicon Nanocrystal–Organic Light-Emitting Devices for Infrared Electroluminescence. Nano Lett. 2010, 10, 1154– 115.
15. Tu, C.-C.; Tang, L.; Huang, J.; Voutsas, A.; Lin, L. Y.; Visible Electroluminescence from Hybrid Colloidal Silicon Quantum Dot-Organic Light-Emitting Diodes, Appl. Phys. Lett. 98, 213102 (2011).
16. Cheng, K.-Y.; Anthony, R.; Kortshagen, U. R.; Holmes, R. J. High-Efficiency Silicon Nanocrystal Light-Emitting Devices. Nano Lett. 2011, 11, 1952– 1956.
17. Puzzo, D. P.; Henderson, E. J.; Helander, M. G.; Wang, Z. B.; Ozin, G. A.; Lu, Z. Visible Colloidal Nanocrystal Silicon Light-Emitting Diode. Nano Lett. 2011, 11, 1585– 1590.
18. Maier-Flaig, F.; Rinck, J.; Stephan, M.; Bocksrocker, T.; Bruns, M.; Kübel, C.; Powell, A. K.; Ozin, G. A.; Uli Lemmer, U. Multicolor Silicon Light-Emitting Diodes (SiLEDs). Nano Lett. 2013, 13, 475–480.
19. Yao, L.; Yu, T.; Ba, L.; Meng, H.; Fang, X.; Wang, Y.; Li, L.; Rong, X.; Wang, S.; Wang, X.; Ran, G.; Pi, X.; Qin, G. Efficient Silicon Quantum Dots Light Emitting Diodes with an Inverted Device Structure, J. Mater. Chem. C, 2016, 4, 673–677.
20. Ghosh, B.; Yamada, H.; Chinnathambi, S.; Ozbilgin, I. N. G.; Shirahata, N. Inverted Device Architecture for Enhanced Performance of Flexible Silicon Quantum Dot Light-Emitting Diode. J. Phys. Chem. Lett. 2018, 9, 5400–5407.
21. Angı, A.; Loch, M.; Sinelnikov, R.; Veinot, J. G. C.; Becherer, M.; Lugli, P.; Rieger, B. The Influence of Surface Functionalization Methods on the Performance of Silicon Nanocrystal LEDs, Nanoscale, 2018, 10, 10337–10342.

22. Liu, X.; Zhao, S.; Gu, W.; Zhang, Y.; Qiao, X.; Ni, Z.; Pi, X.; Yang, D. Light-Emitting Diodes Based on Colloidal Silicon Quantum Dots with Octyl and Phenylpropyl Ligands. ACS Appl. Mater. Interfaces, 2018, 10, 5959–5966.
23. Ghosh, B.; Hamaoka, T.; Nemoto, Y.; Takeguchi, M.; Shirahata, N. Impact of Anchoring Monolayers on the Enhancement of Radiative Recombination in Light-Emitting Diodes Based on Silicon Nanocrystals. J. Phys. Chem. C 2018, 122, 6422– 6430.
24. Zhao, S.; Ni, Z.; Tan, H.; Wang, Y,; Jin, H.; Nie, T.; Xu, M.; Pi, X.; Yang, D. Electroluminescent Synaptic Devices with Logic Functions, Nano Energy 2018, 54, 383-389.
25. Yamada, H.; Shirahata, N. Silicon Quantum Dot Light Emitting Diode at 620 nm, Micromachines 2019, 10, 318.
26. Ghosh, B.; Shirahata, N. All-Inorganic Red-Light Emitting Diodes Based on Silicon Quantum Dots, Crystals 2019, 9, 385.
27. Liu, N.; Huo, K.; McDowell, M. T.; Zhao, J.; Cui, Y. Rice Husks as a Sustainable Source of Nanostructured Silicon for High Performance Li-Ion Battery Anodes. Sci. Rep. 2013, 3, 1–7.